2024 European Control Conference (ECC)
June 25-28, 2024. Stockholm, Sweden

Sensors Placement Analysis and Temperature Estimation in Lithium-Ion Batteries with a Cascaded Electrochemical-Thermal Model

Patryck Ferreira and Shu-Xia Tang

***Abstract*— This study presents a novel thermal model for cylindrical lithium-ion batteries using ten Ordinary Differential Equations (ODEs). The model covers all battery components and focuses on a simplified assembly with eight parts rolled up on a central mandrel and gaps filled with liquid electrolyte. One key input to the thermal model is the thermal power generated in the battery, calculated using a simplified electrochemical Single Particle Model (SPM) with two Partial Differential Equations (PDEs). This leads to a coupled system of 20 ODEs, where 10 ODEs represent the electrochemical model based on Padé approximation method, and 10 ODEs represent the thermal model. Temperature profiles within the battery are estimated using the Luenberger observer, with feasible sensor placement strategies discussed. Simulation results validate the model's accuracy by demonstrating temperature consistency between the thermal model and the Luenberger observer.**

***Index Terms*— Lithium-Ion Batteries, Sensors Placement, Cascaded Electrochemical-Thermal Model, Luenberger Observer, Padé Approximation.**

I. Introduction

Effective monitoring of the internal temperature of lithium-ion batteries (LiBs) is crucial to ensure their safe and efficient operation [1]. Precise temperature estimation within LiBs is a pivotal element in mitigating thermal runaway, enhancing performance, and extending battery life [2]. Thermal management plays a central role in the design and operation of LiBs, given the substantial influence of internal temperature on their performance and safety [3]. Extreme temperature conditions can lead to catastrophic failures, including capacity loss, electrolyte degradation, and other adverse effects when temperatures soar, while efficiency and power output suffer under colder conditions [4]. Accurate temperature measurement in LiBs presents challenges due to their sealed and compact design [5].

In the existing literature, numerous articles address temperature estimation, primarily focusing on the core and/or surface temperatures. For example, [6] models and estimates the average temperature, while [7] and [8] estimate temperature for both the core and surface. Unlike previous studies such as [9] and [10], which considered the entire spiral-wound structure but did not calculate the temperature in each internal part of the battery, this study simplifies the spiral structure to ensure accurate temperature calculations across different parts within the battery.

The contributions of this study are summarized as follows:

- Compared with [11] which only two ODE were employed. This study distinguishes itself by employing a cascaded system comprising nine ODEs for each component within the battery, with an additional ODE dedicated to surface temperature estimation, totaling ten ODEs.
- Compared with [7], which utilized the Equivalent Circuit Model (ECM), this study introduces the use of an electrochemical model for thermal power generation based on the fundamental principles of the battery's electrochemistry.
- Compared to [12], who employed a fourth-order Padé approximation, this article utilizes a fifth-order Padé approximation.
- Unlike the approach in [8], which proposes inserting a sensor internally into the battery, this study explores safer methods of sensor placement. It considers realistic strategies aimed at enhancing battery safety.

The subsequent sections of this article are organized as follows: In Section II, the thermal model is introduced. Subsequently, the article delves into the electrochemical model. Section III covers the implementation of the Luenberger observer for temperature estimation. Section IV presents the simulation results, thereby validating both the thermal model and the Luenberger observer. In Section V, the conclusion is provided along with future research directions.

II. Cascaded Electrochemical-Thermal Model

This section explores the cascaded electrochemical-thermal model, integrating both electrochemical and thermal aspects to comprehensively understand the battery behavior.

A. Thermal Model

A typical cylindrical lithium-ion battery consists of spiral roll cells, as shown in Fig. 1. Its structure involves layers rolled around a central mandrel and inserted into a cylindrical case, with liquid electrolyte filling the gaps between components [10]. The thermal model, depicted in Fig. 1, includes temperature and resistance parameters such as: T_{e} for electrolyte temperature, $T_{\mathrm{c}-}$ and R_{c-} for negative collector, $T_{\mathrm{c}+}$ and R_{c+} for positive collector, T_{s1}, T_{s2}, R_{s1}, and R_{s2} for separator, T_{p1}, T_{p2}, R_{p1}, and R_{p2} for positive electrode, and T_{n1}, T_{n2}, R_{n1}, and R_{n2} for negative electrode. Additionally, T_{c} and R_{c} represent the case, while T_{air} and R_{air} denote air. Thermal power originates from the battery center.

Equation (II.1) is derived from [11], where a thermal model was developed to analyze core and surface temperatures. In this study, Equation (II.1) is used to model the

P. Ferreira and S.-X. Tang (corresponding author) are with the Department of Mechanical Engineering, Texas Tech University, Lubbock, USA. patferre@ttu.edu, shuxia.tang@ttu.edu.

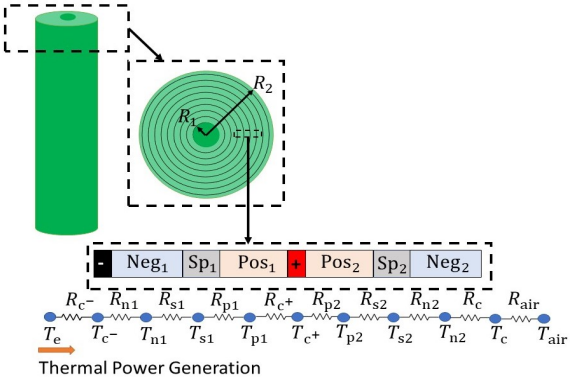

Fig. 1: Thermal-electrochemical schematic.

temperature in different components of the battery.

$$\dot{T}_i(t) = \frac{Q_i(t)}{\rho_i c_{p,i}}, \tag{II.1}$$

where $\dot{T}_i$ represents the rate of temperature change over time, ρ_i denotes the density, $c_{p,i}$ stands for the heat capacity, and Q_i represents the thermal power generated, for $i \in \{\text{e, c}^-\text{, n1, s1, p1 , c}^+\text{, p2, s2, n2 , c , air}\}$.

The thermal power $Q_i(t)$ is normalized by dividing it by the volume v_i, resulting in the unit of measurement W/m^3, and is depicted in (II.2).

$$Q_i(t) = \frac{S(t) + q_{\text{cond},i}(t) + q_{\text{conv},i}(t)}{v_i}. \tag{II.2}$$

Remark 1. *In this paper, $Q_i(t)$ is divided into three components: electrochemical reactions $S(t)$, conduction interaction between components $q_{\text{cond},i}(t)$, and convective heat transfer of the electrolyte, represented as $q_{\text{conv},i}(t)$, for $i \in \{\text{e, c}^-\text{, n1, s1, p1 , c}^+\text{, p2, s2, n2 , c , air}\}$.*

Since $S(t)$ is produced as a function of chemical reactions, it will be discussed in Section II-B. $q_{\text{cond},i}(t)$ is defined as:

$$q_{\text{cond},i}(t) = \frac{\Delta T_i(t)}{R_i},$$

where $\Delta T_i(t)$ denotes the temperature difference in interacting components, and R_i represents the thermal resistance between these components. $q_{\text{conv}}(t)$ is based on the Newton cooling of law and is expressed as follows:

$$q_{\text{conv},i}(t) = hA\Delta T_i(t),$$

where h represents the electrolyte convective heat transfer coefficient, A is the area where the electrolyte is applied, and $\Delta T_i(t)$ is the temperature difference between the electrolyte and each component in contact with the electrolyte, for $i \in \{\text{e, c}^-\text{, n1, s1, p1 , c}^+\text{, p2, s2, n2 , c , air}\}$.

Assumption 1. *This article simplifies the structure of spiral roll cells within a thin layer, considering eight internal components including the electrolyte and casing, totaling ten parts.*

1) Temperature Model for Each Component of the Battery: To construct a thermal model capable of determining the temperature of each of the aforementioned components, a cascade system consisting of 10 ODEs is developed, with each equation corresponding to one of the battery's components.

Electrolyte temperature $T_{\text{e}}(t)$: In the electrolyte, two thermal power components exist: the first one is the electrochemical heat $S(t)$, and the second one is the heat $q_{\text{conv}}(t)$. The temperature of the electrolyte is described by the following equation:

$$\dot{T}_{\text{e}}(t) = \frac{hA(T_{\text{e}}(t) - T_{\text{c}^-}(t))}{\lambda_{\text{e}}} + \frac{S(t)}{\lambda_{\text{e}}},$$

where $\lambda_{\text{e}} = v_{\text{e}}\rho_{\text{e}}c_{\text{pe}}$, with v_{e} representing the volume of the electrolyte in the battery, ρ_{e} denoting the density of the electrolyte, and c_{pe} as the heat capacity of the electrolyte.

Negative collector temperature T_{c^-}: In the negative collector, all heat generation components are present, including $S(t)$ due to electrochemical reactions, q_{cond} resulting from the interaction between the electrolyte and the negative collector, and q_{conv} due to convective heat generated by the electrolyte. The temperature of the negative collector is determined by the following equation:

$$\dot{T}_{\text{c}^-}(t) = \frac{T_{\text{e}}(t) - T_{\text{c}^-}(t)}{\lambda_{\text{c}^-}R_{\text{c}^-}} + \frac{hA(T_{\text{e}}(t) - T_{\text{c}^-}(t))}{\lambda_{\text{c}^-}} + \frac{S(t)}{\lambda_{\text{c}^-}},$$

where $\lambda_{\text{c}^-} = v_{\text{c}^-}\rho_{\text{c}^-}c_{\text{pc}^-}$, with v_{c^-} representing the volume of the negative collector, ρ_{c^-} denoting the density of the negative collector, and c_{pc^-} as the heat capacity of the negative collector.

Similar to the negative collector temperature, equations for the negative electrode, separator, positive electrode, and positive collector can also be derived.

Negative electrode temperature $T_{\text{n1}}(t)$ is as follows:

$$\dot{T}_{\text{n1}}(t) = \frac{T_{\text{c}^-}(t) - T_{\text{n1}}(t)}{\lambda_{\text{n1}}R_{\text{n1}}} + \frac{hA(T_{\text{e}}(t) - T_{\text{n1}}(t))}{\lambda_{\text{n1}}} + \frac{S(t)}{\lambda_{\text{n1}}},$$

where $\lambda_{\text{n1}} = v_{\text{n1}}\rho_{\text{n1}}c_{\text{pn1}}$, with v_{n1} as the volume of the negative electrode, ρ_{n1} as the density of the negative electrolyte, and c_{pn1} as the heat capacity of the negative electrolyte.

Separator temperature $T_{\text{s1}}(t)$ is described as follows:

$$\dot{T}_{\text{s1}}(t) = \frac{T_{\text{n1}}(t) - T_{\text{s1}}(t)}{\lambda_{\text{s1}}R_{\text{s1}}} + \frac{hA(T_{\text{e}}(t) - T_{\text{s1}}(t))}{\lambda_{\text{s1}}} + \frac{S(t)}{\lambda_{\text{s1}}},$$

where $\lambda_{\text{s1}} = v_{\text{s1}}\rho_{\text{s1}}c_{ps1}$, with v_{s1} representing the volume of the separator, ρ_{s1} denoting the density of the separator, and c_{ps1} as the heat capacity of the separator.

Positive electrode $T_{\text{p1}}(t)$ is defined as follows:

$$\dot{T}_{\text{p1}}(t) = \frac{T_{\text{s1}}(t) - T_{\text{p1}}(t)}{\lambda_{\text{p1}}R_{\text{p1}}} + \frac{hA(T_{\text{e}}(t) - T_{\text{p1}}(t))}{\lambda_{\text{p1}}} + \frac{S(t)}{\lambda_{\text{p1}}},$$

where $\lambda_{\text{p1}} = v_{\text{p1}}\rho_p c_{pp1}$, with v_{p1} representing the volume of the positive electrode, ρ_{p1} denoting the density of the positive electrode, and c_{pp1} as the heat capacity of the positive electrode.

Positive collector $T_{\mathrm{c}+}$ is described as follows:

$$\dot{T}_{\mathrm{c}+}(t) = \frac{T_{\mathrm{p1}}(t) - T_{\mathrm{c}+}(t)}{\lambda_{\mathrm{c}+} R_{\mathrm{c}+}} + \frac{hA(T_{\mathrm{e}}(t) - T_{\mathrm{c}+}(t))}{\lambda_{\mathrm{c}+}} + \frac{S(t)}{\lambda_{\mathrm{c}+}},$$

where $\lambda_{\mathrm{c}+} = v_{\mathrm{c}+}\rho_{\mathrm{c}+}c_{p\mathrm{c}+}$, with $v_{\mathrm{c}+}$ representing the volume of the positive collector, $\rho_{\mathrm{c}+}$ denoting the density of the positive collector, and $c_{p\mathrm{c}+}$ as the heat capacity of the positive collector.

Positive electrode $T_{\mathrm{p2}}(t)$, is defined as follows:

$$\dot{T}_{\mathrm{p2}}(t) = \frac{T_{\mathrm{c}+}(t) - T_{\mathrm{p2}}(t)}{\lambda_{\mathrm{p2}} R_{\mathrm{p2}}} + \frac{hA(T_{\mathrm{e}}(t) - T_{\mathrm{p2}}(t))}{\lambda_{\mathrm{p2}}} + \frac{S(t)}{\lambda_{\mathrm{p2}}},$$

where the properties of T_{p2} are the same as those of T_{p1}.

Separator temperature $T_{\mathrm{s2}}(t)$, is described as follows:

$$\dot{T}_{\mathrm{s2}}(t) = \frac{T_{\mathrm{p2}}(t) - T_{\mathrm{s2}}(t)}{\lambda_{\mathrm{s2}} R_{\mathrm{s2}}} + \frac{hA(T_{\mathrm{e}}(t) - T_{\mathrm{s2}}(t))}{\lambda_{\mathrm{s2}}} + \frac{S(t)}{\lambda_{\mathrm{s2}}},$$

where the properties of T_{s2} are the same as those of T_{s1}.

Negative electrode $T_{\mathrm{n2}}(t)$ is as follows:

$$\dot{T}_{\mathrm{n2}}(t) = \frac{T_{\mathrm{s2}}(t) - T_{\mathrm{n2}}(t)}{\lambda_{\mathrm{n2}} R_{\mathrm{n2}}} + \frac{hA(T_{\mathrm{e}}(t) - T_{\mathrm{n2}}(t))}{\lambda_{\mathrm{n2}}} + \frac{S(t)}{\lambda_{\mathrm{n2}}},$$

where the properties of T_{n2} are the same as those of T_{n1}.

Case surface temperature $T_{\mathrm{c}}(t)$, is defined as follows: The minus sign in $T_{\mathrm{c}}(t)$ indicates heat extraction from the battery during the interaction between the inner of the battery and the case surface. Conversely, when considering the interaction between the case surface and the air, heat is added to the surface, as follows:

$$\dot{T}_{\mathrm{c}}(t) = \frac{T_{\mathrm{air}}(t) - T_{\mathrm{c}}(t)}{\lambda_{\mathrm{air}} R_{\mathrm{air}}} - \frac{T_{\mathrm{n2}}(t) - T_{\mathrm{c}}(t)}{\lambda_{\mathrm{air}} R_{\mathrm{c}}},$$

where $\lambda_{\mathrm{air}} = v_{\mathrm{air}}\rho_{\mathrm{air}}c_{p\mathrm{air}}$, with v_{air} as the volume of the air in contact with the battery, ρ_{air} as the density of air, $c_{p\mathrm{air}}$ as the heat capacity of air, and R_{c} is the thermal resistance of the case.

2) State-Space System for Thermal Model: The electrochemical-thermal state-space representation of the system is:

$$\begin{aligned} \dot{\mathbf{T}}(t) &= \mathcal{A}\mathbf{T}(t) + \mathcal{B}\mathbf{u}(t), \\ \mathbf{y}(t) &= \mathcal{C}\mathbf{T}(t), \end{aligned}$$

where $\mathbf{T}(t)$ denotes the state vector of the system's temperature, $\mathcal{A}$, $\mathbf{T}(t)$, $\mathcal{B}$ are shown in (II.3), (II.4), and (II.5). The selection of $\mathcal{C}$ is discussed in (III-.1). The input $\mathbf{u}$ is described as follows:

$$\mathbf{u}(t) = \begin{bmatrix} T_{\mathrm{air}}(t) & S(t) \end{bmatrix}^{\mathrm{tr}}.$$

Here, $T_{\mathrm{air}}(t)$ represents the air temperature, and $S(t)$ denotes the thermal power.

B. Thermal Power S(t) derived from Electrochemical model

The result of multiplying current and voltage informs us about the number of electrons moving through a system, along with the energy each electron expends as heat, ultimately providing the total heat production [13]. Electrochemical thermal power is expressed as:

$$S(t) = V(t)I(t).$$

Here, $V(t)$ represents the voltage calculated using the electrochemical model, $I(t)$ is the current applied to the battery.

1) Electrochemical PDE model: This article employs the Single Particle Model (SPM) in its electrochemical model. The lithium concentration in the solid phase, and consequently the concentration of lithium-ions in the active material, follows Fick's law of diffusion [14].

$$\begin{aligned} \frac{\partial c_s^{\pm}}{\partial t}(t, r_s) &= \frac{1}{r_s^2}\frac{\partial}{\partial r_s}\left[D_s^{\pm}(T(t)) r_s^2 \frac{\partial c_s^{\pm}}{\partial r_s}(t, r_s)\right], \\ & \qquad t > 0, \quad r_s \in (0, R_s^{\pm}), \\ \frac{\partial c_s^{\pm}}{\partial r_s}(t, 0) &= 0, \quad t > 0, \\ \frac{\partial c_s^{\pm}}{\partial r_s}(t, R_s^{\pm}) &= -\frac{1}{D_s^{\pm}(T(t))} j^{\pm}(t), \quad t > 0, \\ c_s^{\pm}(0, r_s) &= c_{s,0}^{\pm}(r_s), \quad r_s \in [0, R_s^{\pm}], \end{aligned}$$

where the temporal variable is t, the spatial variable is r_s. The solid phase $c_s^{\pm} \in \mathbb{R}$. $D_s^{\pm}$ is the diffusion coefficient of the solid phase. $j^{\pm}$ is the molar flux given by:

$$j^{+}(t) = -\frac{I(t)}{a_{\mathrm{s}}^{+} F L^{+}}, \quad j^{-}(t) = \frac{I(t)}{a_{\mathrm{s}}^{-} F L^{-}},$$

where $I(t)$ represents the current, $a_s^{\pm}$ stands for the interfacial surface area, F denotes the Faraday constant, and $L^{\pm}$ corresponds to the length of the positive or negative electrode.

Assumption 2. *The diffusion coefficients $D_s^{\pm}$ are assumed constant.*

The voltage is the difference between solid electric potentials at the positive and negative electrodes, given by:

$$V(t) = \phi_s^{+}(t) - \phi_s^{-}(t),$$

where the solid electric potentials are given as follows:

$$\phi_s^{\pm}(t) = \eta^{\pm}(t) + U^{\pm}\left(c_{ss}^{\pm}(t), T(t)\right) + F R_f^{\pm}(T(t)) j^{\pm}(t).$$

In this context, $\eta^{\pm}(t)$ represents the overpotential, $U^{\pm}\left(c_{ss}^{\pm}(t), T(t)\right)$ is the equilibrium potential, specific to the battery in question and discussed in the simulation results section, F denotes the Faraday constant, and $R_f^{\pm}(T(t))$ signifies the resistance.

The reaction overpotential $\eta^{\pm}$ is defined as:

$$\eta^{\pm}(t) = \frac{RT(t)}{\alpha F} \sinh^{-1}\left(\frac{F}{2i_0^{\pm}(t)} j^{\pm}(t)\right),$$

where R represents the gas constant, T denotes the temperature, α signifies the transfer coefficient, and $i_0^{\pm}$ is expressed as [15]:

$$i_0^{\pm}(t) = k^{\pm}\left[c_{ss}^{\pm}(t)\right]^{\alpha_{\mathrm{c}}}\left[c_{\mathrm{e},0}\left(c_{\mathrm{s}}^{\pm,\max} - c_{\mathrm{ss}}^{\pm}(t)\right)\right]^{\alpha_{\mathrm{a}}},$$

where k is the kinetic reaction rate $c_{ss}^{\pm} \triangleq c_s^{\pm}$ represents the boundary concentration in the positive and negative electrodes, and $c_{e,0}$ is the equilibrium electrolyte concentration.

$$\mathcal{A}=\begin{bmatrix}
\frac{hA}{\lambda_{\mathrm{e}}} & -\frac{hA}{\lambda_{\mathrm{e}}} & 0 & 0 & 0 & 0 & 0 & 0 & 0 & 0\\
\frac{hAR_{\mathrm{c}-}-1}{\lambda_{\mathrm{c}-}R_{\mathrm{c}-}} & -\frac{hAR_{\mathrm{c}-}+1}{\lambda_{\mathrm{c}-}R_{\mathrm{c}-}} & 0 & 0 & 0 & 0 & 0 & 0 & 0 & 0\\
\frac{hA}{\lambda_{\mathrm{n1}}} & \frac{1}{\lambda_{\mathrm{n1}}R_{\mathrm{n1}}} & \frac{-hAR_{\mathrm{n1}}-1}{\lambda_{\mathrm{n1}}R_{\mathrm{n1}}} & 0 & 0 & 0 & 0 & 0 & 0 & 0\\
\frac{hA}{\lambda_{\mathrm{s1}}} & 0 & \frac{1}{\lambda_{\mathrm{s1}}R_{\mathrm{s1}}} & \frac{-hAR_{\mathrm{s1}}-1}{\lambda_{\mathrm{s1}}R_{\mathrm{s1}}} & 0 & 0 & 0 & 0 & 0 & 0\\
\frac{hA}{\lambda_{p1}} & 0 & 0 & \frac{1}{\lambda_{\mathrm{p1}}R_{\mathrm{p1}}} & \frac{-hAR_{\mathrm{p1}}-1}{\lambda_{\mathrm{p1}}R_{\mathrm{p1}}} & 0 & 0 & 0 & 0 & 0\\
\frac{hA}{\lambda_{\mathrm{c}+}} & 0 & 0 & 0 & \frac{1}{\lambda_{\mathrm{c}+}R_{\mathrm{c}+}} & \frac{-hAR_{\mathrm{c}+}-1}{\lambda_{\mathrm{c}+}R_{\mathrm{c}+}} & 0 & 0 & 0 & 0\\
\frac{hA}{\lambda_{\mathrm{p2}}} & 0 & 0 & 0 & 0 & \frac{1}{\lambda_{\mathrm{p2}}R_{\mathrm{p2}}} & \frac{-hAR_{\mathrm{p2}}-1}{\lambda_{\mathrm{p2}}R_{\mathrm{p2}}} & 0 & 0 & 0\\
\frac{hA}{\lambda_{\mathrm{s2}}} & 0 & 0 & 0 & 0 & 0 & \frac{1}{\lambda_{\mathrm{s2}}R_{\mathrm{s2}}} & \frac{-hAR_{\mathrm{s2}}-1}{\lambda_{\mathrm{s2}}R_{\mathrm{s2}}} & 0 & 0\\
\frac{hA}{\lambda_{\mathrm{n2}}} & 0 & 0 & 0 & 0 & 0 & 0 & \frac{1}{\lambda_{\mathrm{n2}}R_{\mathrm{n2}}} & \frac{-hAR_{\mathrm{n2}}-1}{\lambda_{\mathrm{n2}}R_{\mathrm{n2}}} & 0\\
0 & 0 & 0 & 0 & 0 & 0 & 0 & 0 & \frac{1}{\lambda_{\mathrm{air}}R_{\mathrm{air}}} & \frac{-R_{\mathrm{air}}-R_{\mathrm{c}}}{\lambda_{\mathrm{air}}R_{\mathrm{c}}}
\end{bmatrix}, \tag{II.3}$$

$$\mathbf{T}(t)=\begin{bmatrix}T_{\mathrm{e}}(t) & T_{\mathrm{c}-}(t) & T_{\mathrm{n1}}(t) & T_{\mathrm{s1}}(t) & T_{\mathrm{p1}}(t) & T_{\mathrm{c}+}(t) & T_{\mathrm{p2}}(t) & T_{\mathrm{s2}}(t) & T_{\mathrm{n2}}(t) & T_{\mathrm{c}}(t)\end{bmatrix}^{\mathrm{tr}}, \tag{II.4}$$

$$\mathcal{B}=\begin{bmatrix}
0 & 0 & 0 & 0 & 0 & 0 & 0 & 0 & 0 & \frac{-1}{\lambda_{\mathrm{air}}R_{\mathrm{air}}}\\
\frac{1}{\lambda_{\mathrm{e}}} & \frac{1}{\lambda_{\mathrm{c}-}} & \frac{1}{\lambda_{\mathrm{n1}}} & \frac{1}{\lambda_{\mathrm{s1}}} & \frac{1}{\lambda_{\mathrm{p1}}} & \frac{1}{\lambda_{\mathrm{c}+}} & \frac{1}{\lambda_{\mathrm{p2}}} & \frac{1}{\lambda_{\mathrm{s2}}} & \frac{1}{\lambda_{\mathrm{n2}}} & 0
\end{bmatrix}^{\mathrm{tr}}, \tag{II.5}$$

2) Reduced-Order Electrochemical Model: The article applies the Padé approximation method to linearize the model, calculated using the code *pade* on Wolfram Alpha. The transcendental transfer functions for the electrodes are:

$$\frac{C_s^{\pm}(s)}{I(s)}=\frac{R_s^{\pm}-R_s^{\pm}e^{2R_s^{\pm}\sqrt{s/D_s^{\pm}}}}{D_s^{\pm}AFL\left(R_s^{\pm}\sqrt{\frac{s}{D_s^{\pm}}}+e^{2R\sqrt{s/D_s^{\pm}}}\left(R_s^{\pm}\sqrt{\frac{s}{D_s^{\pm}}}-1\right)+1\right)}.$$

The transcendental transfer functions are extended to the 5th order using the Padé approximation method to estimate the concentration in the solid electrode, expressed as follows:

$$\frac{C_s^{\pm}(s)}{I(s)}=\frac{N^5(s)}{D^5(s)},$$

where

$$\begin{aligned}N^5(s)&=\pm\frac{R_s^{\pm 7}s^4}{3968055D_s^{\pm 4}AFL}\pm\frac{4R_s^{\pm 5}s^3}{33915D_s^{\pm 3}AFL}\\&\pm\frac{21R_s^{\pm 3}s^2}{1615D_s^{\pm 2}AFL}\pm\frac{8R_s^{\pm}s}{19D_s^{\pm}AFL}\pm\frac{3}{R_s^{\pm}AFL},\\D^5(s)&=\frac{R_s^{\pm 8}s^5}{218243025D_s^{\pm 4}}+\frac{2R_s^{\pm 6}s^4}{305235D_s^{\pm 3}}+\frac{3R_s^{\pm 4}s^3}{2261D_s^{\pm 2}}\\&+\frac{7R_s^{\pm 2}s^2}{95D_s^{\pm}}+s.\end{aligned}$$

When calculating C^+, all numerator terms are negative, while for C^-, all numerator terms are positive.

This results in a coupled system of 20 ODEs: 10 for the electrochemical model and 10 for the thermal model.

III. Luenberger Observer

The Luenberger observer takes the available output measurements and uses them to estimate the internal states of the actual system. The Luenberger observer is given by [16]:

$$\dot{\hat{\mathbf{T}}}(t)=\mathcal{A}\hat{\mathbf{T}}(t)+\mathcal{B}\mathbf{u}(t)+L[\mathcal{C}\mathbf{T}(t)-\mathcal{C}\hat{\mathbf{T}}(t)], \tag{III.1}$$

where $\mathcal{A}$, $\mathcal{B}$, and $\mathcal{C}$ are model parameters, and L is the observer gain. The error between the estimated state and the actual state is defined as $\tilde{\mathbf{T}}(t)=\mathbf{T}(t)-\hat{\mathbf{T}}(t)$. In terms of this definition, the error dynamics $\dot{\tilde{\mathbf{T}}}(t)$ is derived as follows:

$$\dot{\tilde{\mathbf{T}}}(t)=(\mathcal{A}-L\mathcal{C})\tilde{\mathbf{T}}(t). \tag{III.2}$$

1) Observability Analysis and Realistic Sensor Placement: A Matlab code was developed to simulate all possible observability configurations for placing two sensors on the battery. Since there are 2 sensors, and for each sensor, there are 10 choices for sensor placement for each measurement, there are a total of $\mathcal{C}_{10}^2=45$ combinations of $\mathcal{C}$ matrices, each with a size of 2×10. However, upon checking the observability Grammian of these combinations, only 6 of them are observable.

In the context of the matrices given by equations (III.3), (III.4), (III.5), (III.6), (III.7), and (III.8), each matrix represents the placement of a sensor within a specific region of a larger system.

In (III.3), sensors are placed in the negative electrode and outside the case. However, it is worth noting that installing sensors in the negative electrode is quite challenging; for this reason, this matrix configuration was disregarded:

$$\mathcal{C}([3;10])=\begin{bmatrix}0&0&1&0&0&0&0&0&0&0\\0&0&0&0&0&0&0&0&0&1\end{bmatrix}. \tag{III.3}$$

In (III.4) and (III.5), the sensors are situated in the separator and positioned outside the case. Similar to the previous case, it is worth noting that placing sensors in the separator presents a challenging task, which resulted in the exclusion of these matrix configurations:

$$\mathcal{C}([4;10])=\begin{bmatrix}0&0&0&1&0&0&0&0&0&0\\0&0&0&0&0&0&0&0&0&1\end{bmatrix}, \tag{III.4}$$

$$\mathcal{C}([8;10])=\begin{bmatrix}0&0&0&0&0&0&0&1&0&0\\0&0&0&0&0&0&0&0&0&1\end{bmatrix}. \tag{III.5}$$

In (III.6) and (III.7), the sensors are located in the positive electrode and positioned outside the case. Once more, it is

emphasized that installing sensors in the positive electrode is a complex undertaking, leading to the rejection of these matrix configurations:

$$\mathcal{C}([5;10]) = \begin{bmatrix} 0 & 0 & 0 & 0 & 1 & 0 & 0 & 0 & 0 & 0 \\ 0 & 0 & 0 & 0 & 0 & 0 & 0 & 0 & 0 & 1 \end{bmatrix}, \quad \text{(III.6)}$$

$$\mathcal{C}([7;10]) = \begin{bmatrix} 0 & 0 & 0 & 0 & 0 & 0 & 1 & 0 & 0 & 0 \\ 0 & 0 & 0 & 0 & 0 & 0 & 0 & 0 & 0 & 1 \end{bmatrix}. \quad \text{(III.7)}$$

In contrast, (III.8) represents a matrix with sensors positioned outside on the tab of the positive collector and case. This configuration is considered a more feasible and practical choice due to the simple installation process:

$$\mathcal{C}([6;10]) = \begin{bmatrix} 0 & 0 & 0 & 0 & 0 & 1 & 0 & 0 & 0 & 0 \\ 0 & 0 & 0 & 0 & 0 & 0 & 0 & 0 & 0 & 1 \end{bmatrix}. \quad \text{(III.8)}$$

2) Observer design: This section explores observer design for a specific system, with a focus on selecting the observer gain matrix to ensure convergence.

Theorem 1. *Consider the system (II.3)-(II.5), the observer* (III.1)*, and the matrix C* (III.8)*. Choose the observer gain matrix $L \in \mathbb{R}^{10\times 2}$ such that $\mathcal{A} - L\mathcal{C}$ is Hurwitz. For any initial conditions $\mathbf{T}(0)$ and $\hat{\mathbf{T}}(0)$, and any input $\mathbf{u}(t)$, the error between the observer's estimated state $\hat{\mathbf{T}}(t)$ and the actual system state $\mathbf{T}(t)$ converges exponentially to zero in the sense that:*

$$\|\tilde{T}(t)\| \leq \|\tilde{T}(0)\| e^{-\frac{\lambda_{\min}(Q)}{2\lambda_{\max}(P)}t} \sqrt{\frac{\lambda_{\max}(P)}{\lambda_{\min}(P)}}.$$

Proof. Choose the Lyapunov function as follows:

$$V(\tilde{\mathbf{T}}(t)) = \tilde{\mathbf{T}}(t)^{\text{tr}} P \tilde{\mathbf{T}}(t), \quad \text{(III.9)}$$

where P is the solution of the equation:

$$(\mathcal{A} - L\mathcal{C})^{\text{tr}} P + P(\mathcal{A} - L\mathcal{C}) = -Q,$$

for a positive definite matrix Q. Based on Lyapunov theorem, P is positive definite. Based on (III.9), we have:

$$\lambda_{\min}(P)\|\tilde{T}(t)\|_2^2 \leq V(\tilde{T}(t)) \leq \lambda_{\max}(P)\|\tilde{T}(t)\|_2^2. \quad \text{(III.10)}$$

The time derivative of $V(\tilde{\mathbf{T}}(t))$ is:

$$\begin{aligned} \dot{V}(\tilde{\mathbf{T}}(t)) &= \frac{d}{dt}(\tilde{\mathbf{T}}(t)^{\text{tr}} P \tilde{\mathbf{T}}(t)) \\ &= \dot{\tilde{\mathbf{T}}}(t)^{\text{tr}} P \tilde{\mathbf{T}}(t) + \tilde{\mathbf{T}}(t)^{\text{tr}} P \dot{\tilde{\mathbf{T}}}(t). \end{aligned} \quad \text{(III.11)}$$

By substituting the error dynamics (III.2), and using (III.10), the Equation (III.11) becomes:

$$\begin{aligned} \dot{V}(\tilde{\mathbf{T}}(t)) &= \tilde{\mathbf{T}}(t)^{\text{tr}}(\mathcal{A} - L\mathcal{C})^{\text{tr}} P \tilde{\mathbf{T}}(t) \\ &\quad + \tilde{\mathbf{T}}(t)^{\text{tr}} P(\mathcal{A} - L\mathcal{C})\tilde{\mathbf{T}}(t) \\ &= -\tilde{\mathbf{T}}(t)^{\text{tr}} Q \tilde{\mathbf{T}}(t) \leq -\lambda_{\min}(Q)\|\tilde{\mathbf{T}}(t)\|_2^2 \\ &\leq \frac{-\lambda_{\min}(Q)}{\lambda_{\max}(P)} V(\tilde{\mathbf{T}}(t)). \end{aligned}$$

Applying the comparison principle, the following equation was obtained:

$$V(\tilde{\mathbf{T}}(t)) \leq V(\tilde{\mathbf{T}}(0)) e^{-\frac{\lambda_{\min}(Q)}{\lambda_{\max}(P)}t},$$

which completes the proof. □

IV. Simulation Results

The simulation was performed using MATLAB on a personal computer from Samsung equipped with an Intel i5-10210U 1.6 GHz CPU and 31.8 GB of RAM.

The equilibrium potential of the active materials in the positive and negative electrodes is denoted as U^+ and U^-, respectively. The equilibrium potential for the positive and negative electrodes has the following expressions [17]:

$$\begin{aligned} U^+(\theta^+) &= 0.6379 + 0.5416e^{-305.5309\theta^+} \\ &+ 0.044\tanh\left(-\frac{\theta^+ - 0.1958}{0.1088}\right) - 0.1978\tanh\left(\frac{\theta^+ - 1.0571}{0.0854}\right) \\ &- 0.6875\tanh\left(\frac{\theta^+ - 0.0117}{0.0529}\right) - 0.0175\tanh\left(\frac{\theta^+ - 0.5692}{0.0875}\right), \\ U^-(\theta^-) &= 3.4323 - 0.4828e^{-80.2493(1-\theta^-)^{1.3108}} \\ &- 3.2474\times 10^{-6} e^{20.2645(1-\theta^-)^{3.8003}} \\ &+ 3.2482\times 10^{-6} e^{20.2645(1-\theta^-)^{3.7005}}, \end{aligned}$$

where $\theta^{\pm} = \frac{c_{s\pm}(R_{\pm},t)}{c_s \max} \times 100\%$. The thermal resistances for the collector, electrode, separator, and case are calculated using the formula: $R_{\text{cond}} = \frac{\ln(r_2/r_1)}{2\pi kL}$, where r_2 and r_1 represent the external and internal radius, L is the length, and k is the thermal conductivity. For the electrolyte and air, the thermal resistance is determined by: $R_{\text{conv}} = \frac{1}{2\pi rhL}$, where r, h, and L denote the radius, convective heat transfer coefficient, and length, respectively [18, Chapter 3].

The battery, a $LiFePO_4$ 26650 with a capacity of 2560mAh, was initially set to 25°C for both internal and external temperatures to begin with a resting start. The Urban Dynamometer Driving Schedule current profile (UDDS) shown in Fig. 2 is utilized in the electrochemical model, following a C-rate of 1, as recommended for this battery. Detailed electrochemical and thermal properties can be found in [17] and [19].

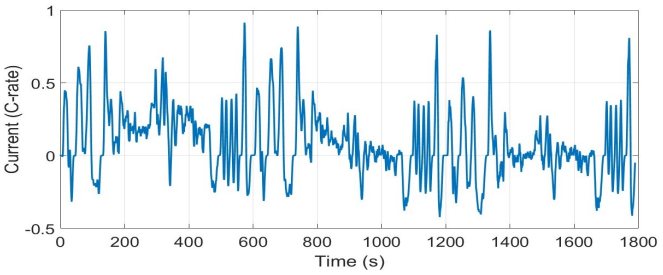

Fig. 2: UDDS current profile.

In Fig. 3, the internal temperatures of the battery and the case temperature are presented. The highest internal temperature, specifically at the negative electrode (T_{n2}), was recorded at 57.96°C, occurring after 938 seconds of monitoring. Beyond this point, internal temperatures remained relatively consistent. After 1300 seconds (the dashed line in Fig. 3), the electrolyte temperature started to increase and reached a peak of 55.48°C at exactly 1770 seconds. This notable increase in electrolyte temperature may indicate the

beginning of a thermal runaway event. The case temperature was measured at 42.97°C.

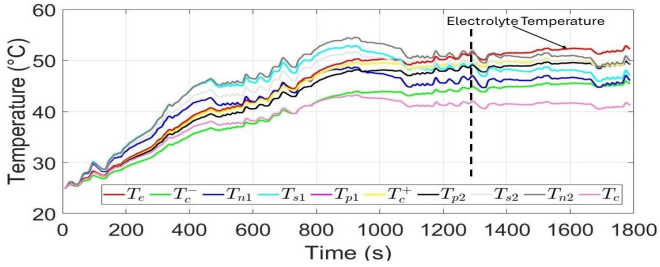

Fig. 3: Battery temperatures.

In all simulation scenarios, the Luenberger observer was initialized at 0°C, and the poles were set to -1.1, -0.00391, -0.00904, -0.02, -0.4599, -0.01, -0.004, -0.004, -0.0000009, and -0.0005. Fig. 4 illustrates the error dynamics between the thermal model and the Luenberger observer, demonstrating the accuracy of the observer's estimations compared to the thermal model.

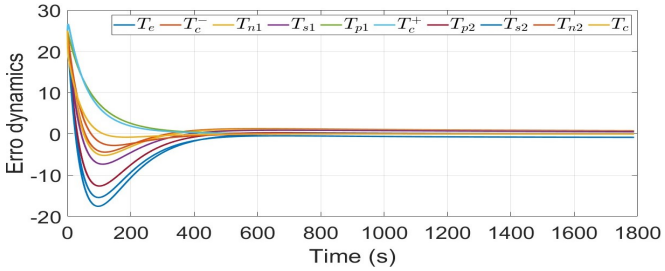

Fig. 4: Error dynamics.

Fig. 5 shows the 2-norm of the observer error approaches zero within 600 seconds.

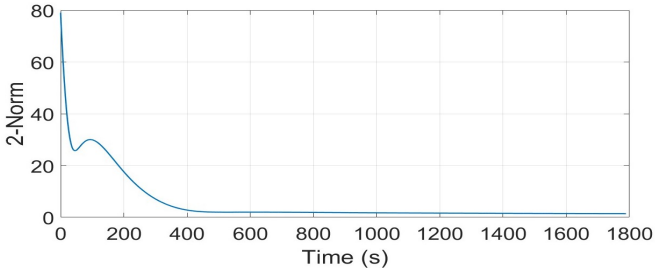

Fig. 5: $\|\mathbf{T}(t) - \hat{\mathbf{T}}(t)\|_2$.

V. Conclusion and Future Work

In this article, a new thermal model is presented for accurate temperature estimation of internal components in cylindrical batteries. The model integrates conduction, convection, and electrochemical reactions for heat generation efficiently. Simulations validate its effectiveness, and comparing it with the Luenberger observer improves reliability. Future work involves developing PDE-based models. Additionally, multiple windings within the spiral will be taken into consideration within the battery, and adaptive observers will be developed to deal with model uncertainties.

Acknowledgments

The authors acknowledge Mark Sewkarran for his preliminary study on Padé approximation in this paper. We thank Dr. Xinfan Lin for his valuable suggestions regarding potential future work.

References

[1] Yuqing Chen, Yuqiong Kang, Yun Zhao, Li Wang, Jilei Liu, Yanxi Li, Zheng Liang, Xiangming He, Xing Li, Naser Tavajohi, et al. A review of lithium-ion battery safety concerns: The issues, strategies, and testing standards. *Journal of Energy Chemistry*, 59:83–99, 2021.

[2] Bruce Dunn, Haresh Kamath, and Jean-Marie Tarascon. Electrical energy storage for the grid: a battery of choices. *Science*, 334(6058):928–935, 2011.

[3] Liange He, Zihan Gu, Yan Zhang, Haodong Jing, and Pengpai Li. Review on thermal management of lithium-ion batteries for electric vehicles: Advances, challenges, and outlook. *Energy & Fuels*, 37(7):4835–4857, 2023.

[4] Xinghui Zhang, Zhao Li, Lingai Luo, Yilin Fan, and Zhengyu Du. A review on thermal management of lithium-ion batteries for electric vehicles. *Energy*, 238:121652, 2022.

[5] Ala A Hussein. Sensorless temperature estimation for li-ion battery cells: An overview, practical considerations, challenges and future trends. *IEEE Transactions on Industry Applications*, 2023.

[6] Shu-Xia Tang, Leobardo Camacho-Solorio, Yebin Wang, and Miroslav Krstic. State-of-charge estimation from a thermal–electrochemical model of lithium-ion batteries. *Automatica*, 83:206–219, 2017.

[7] Xinfan Lin, Anna G Stefanopoulou, Hector E Perez, Jason B Siegel, Yonghua Li, and R Dyche Anderson. Quadruple adaptive observer of the core temperature in cylindrical li-ion batteries and their health monitoring. In *2012 American Control Conference (ACC)*, pages 578–583. IEEE, 2012.

[8] Xinfan Lin, Hector E Perez, Jason B Siegel, Anna G Stefanopoulou, Yonghua Li, R Dyche Anderson, Yi Ding, and Matthew P Castanier. Online parameterization of lumped thermal dynamics in cylindrical lithium-ion batteries for core temperature estimation and health monitoring. *IEEE Transactions on Control Systems Technology*, 21(5):1745–1755, 2012.

[9] Ngoc Tham Tran, Troy Farrell, Mahinda Vilathgamuwa, Yang Li, et al. A computationally efficient coupled electrochemical-thermal model for large format cylindrical lithium ion batteries. *Journal of The Electrochemical Society*, 166(13):A3059, 2019.

[10] Xiongwen Zhang. Thermal analysis of a cylindrical lithium-ion battery. *Electrochimica Acta*, 56(3):1246–1255, 2011.

[11] Chanwoo Park and Arun K Jaura. Dynamic thermal model of li-ion battery for predictive behavior in hybrid and fuel cell vehicles. Technical report, SAE Technical Paper, 2003.

[12] Shifei Yuan, Lei Jiang, Chengliang Yin, Hongjie Wu, and Xi Zhang. A transfer function type of simplified electrochemical model with modified boundary conditions and Padé approximation for li-ion battery: Part 1. lithium concentration estimation. *Journal of Power Sources*, 352:245–257, 2017.

[13] Alexandra Von Meier. *Electric power systems: a conceptual introduction*. John Wiley & Sons, 2006.

[14] Nalin A Chaturvedi, Reinhardt Klein, Jake Christensen, Jasim Ahmed, and Aleksandar Kojic. Algorithms for advanced battery-management systems. *IEEE Control systems magazine*, 30(3):49–68, 2010.

[15] Scott J Moura, Federico Bribiesca Argomedo, Reinhardt Klein, Anahita Mirtabatabaei, and Miroslav Krstic. Battery state estimation for a single particle model with electrolyte dynamics. *IEEE Transactions on Control Systems Technology*, 25(2):453–468, 2016.

[16] Robert L Williams, Douglas A Lawrence, et al. *Linear state-space control systems*. John Wiley & Sons, 2007.

[17] J. Chiew, C. S. Chin, W. D. Toh, Z. Gao, J. Jia, and C. Z. Zhang. A pseudo three-dimensional electrochemical-thermal model of a cylindrical $LiFePO_4$-graphite battery. *Applied Thermal Engineering*, 147:450–463, 2019.

[18] Theodore L Bergman, Adrienne S Lavine, Frank P Incropera, and David P DeWitt. *Introduction to heat transfer*. John Wiley & Sons, 2011.

[19] M. Shadman Rad, Dmitri L. Danilov, Morteza Baghalha, Mohammad Kazemeini, and Peter HL Notten. Thermal modeling of cylindrical $LiFePO_4$ batteries. *Journal of Modern Physics*, 4:1–7, 2013.